Intermetallics 148 (2022) 107613

Contents lists available at ScienceDirect

Intermetallics

journal homepage: www.elsevier.com/locate/intermet

Role of antisite disorder in the martensitic transition of $Ni_{2-x}Mn_{1+x}Ga$

S.V. Malik [a], E.T. Dias [a], V. Srihari [b], P.D. Babu [c], K.R. Priolkar [a,*]

[a] School of Physical and Applied Sciences, Goa University, Taleigao Plateau, Goa, 403 206, India
[b] High Pressure and Synchrotron Radiation Physics Division, Bhabha Atomic Research Centre, Mumbai, 400 085, India
[c] UGC-DAE Consortium for Scientific Research, Mumbai Centre, BARC Campus, Mumbai, 400 085, India

ARTICLE INFO

Keywords:
Mn_2NiGa
Martensite transformation
Heusler alloys

ABSTRACT

A systematic investigation of the structure and local structure of $Ni_{2-x}Mn_{1+x}Ga$ alloys $0 \leq x \leq 1$ reveals antisite disorder to be a possible reason for higher martensitic transformation temperature of Mn_2NiGa as compared to Ni_2MnGa. The antisite disorder between the Y and Z sublattices of the X_2YZ Heusler structure results in segregation of Mn_3Ga type defect phase and a Ni-rich Heulser phase with a higher e/a ratio. This Ni-rich Heusler phase appears to be responsible for the higher martensitic transformation temperature of the Mn_2NiGa type Heusler alloys.

1. Introduction

Mn_2NiGa has attracted attention due its high ferrimagnetic ordering temperature, $T_C = 588$ K and a martensitic transformation at $T_M \approx 270$ K. It presents a large ($\sim$ 4%) magnetic field induced strain (MFIS) caused by a rearrangement of martensitic twins in the presence of the magnetic field [1] and a large inverse magnetocaloric effect [2]. Further, a spin-valve like magnetoresistance is noted at room temperature due to the formation of ferromagnetic nanoclusters in bulk lattice as a result of site occupancy disorder [3]. Antisite disorder in stoichiometric and off-stoichiometric Mn_2NiGa is also believed to be responsible for positive exchange bias which is critical for building nanodevices based on shape memory alloys [4].

Mn_2NiGa is reported to crystallize in the so-called $L2_1B$ or the inverse Heusler structure (XX'YZ) in the austenitic phase. Here, the Y (0,0,0) and Z ($\frac{1}{2}, \frac{1}{2}, \frac{1}{2}$) sites are occupied by Mn and Ga respectively and the X ($\frac{1}{4}, \frac{1}{4}, \frac{1}{4}$) and X' ($\frac{3}{4}, \frac{3}{4}, \frac{3}{4}$) occupied by Ni and Mn atoms with equal probability [5]. However, ab initio calculations have not been able to satisfactorily calculate the properties of Mn_2NiGa using this structure and have used alternate Hg_2CuTi structure [6,7]. The main reason for this failure of theoretical calculations is the presence of antisite disorder in these Mn-rich alloy compositions. In fact, first principle calculations incorporating antisite disorder have indicated significantly large magnetic moments in the high temperature phase of Mn_2NiGa [8].

Ni_2MnGa, on the other hand, has well ordered $L2_1$ face centred cubic austenitic structure and a ferromagnetic ordering temperature $\sim$ 370 K [9]. It transforms from the austenitic state to incommensurate 5M modulated orthorhombic structure at $T_M \approx 220$ K [10]. The transformation temperature, crystal structure as well as the properties of the Ni–Mn-Ga alloys are sensitively dependent on the average valence electron per atom (e/a) ratio [11]. The martensitic structure changes to commensurate 5M for $Ni_{1.95}Mn_{1.19}Ga_{0.86}$ to incommensurate 7M in $Ni_{2.15}Mn_{0.85}Ga$ [12,13]. Electronic structure calculations and extended x-ray absorption fine structure (EXAFS) studies highlight the importance of Ni 3*d* and Ga 4*p* hybrid states at the Fermi level in the martensitic state [14,15]. The hybridization strengthens with the increasing e/a ratio and leads to a proportionate increase in the martensitic transformation temperature from 220 K in Ni_2MnGa to well above the room temperature and even past its T_C.

The e/a ratio for the stoichiometric Ni_2MnGa alloy is 7.5 and can be increased by substituting Ni in place of Mn or Ga or both or by favorably altering the ratio of Mn to Ga. A strong correlation is observed between T_M and the e/a ratio and gives an impression of the e/a ratio being the sole controlling factor of martensitic transformation temperature in Ni–Mn-Ga alloys [11]. However, some prominent exceptions to this so-called e/a rule exist and are related to the inverse Heusler alloy, Mn_2NiGa [1,16]. Though the e/a ratio of Mn_2NiGa is less than that of Ni_2MnGa, it undergoes a martensitic transformation at a temperature ($T_M = 270$ K) higher than that of Ni_2MnGa.

The martensitic structure of Mn_2NiGa is also controversial. While the first report indicated the martensitic structure to be non modulated tetragonal [17], the subsequent neutron diffraction studies reported the martensitic structure as seven-fold modulated orthorhombic [5]. Modulated structures realize due to periodic displacement of atoms from

* Corresponding author.
E-mail address: krp@unigoa.ac.in (K.R. Priolkar).

https://doi.org/10.1016/j.intermet.2022.107613
Received 23 January 2022; Received in revised form 18 April 2022; Accepted 24 May 2022
Available online 18 June 2022

Table 1
e/a ratio calculated from the nominal composition, EDX composition, lattice parameter, a estimated from Rietveld refinement of the XRD patterns (errors in the last digit are given in parenthesis) and the martensitic start temperature, M_s for $Ni_{2-x}Mn_{1+x}Ga$ series.

Alloy	e/a ratio	EDX composition	a Å	M_s (K)
Ni_2MnGa RQ	7.5	$Ni_{2.03}Mn_{1.01}Ga_{0.97}$	5.8240(3)	197
$Ni_{1.75}Mn_{1.25}Ga$ RQ	7.31	$Ni_{1.8}Mn_{1.24}Ga_{0.96}$	5.8456(4)	81
$Ni_{1.5}Mn_{1.5}Ga$ RQ	7.13	$Ni_{1.49}Mn_{1.53}Ga_{0.98}$	5.8624(2)	NM
$Ni_{1.25}Mn_{1.75}Ga$ RQ	6.94	$Ni_{1.24}Mn_{1.8}Ga_{0.96}$	5.8818(3)	NM
$Ni_{1.25}Mn_{1.75}Ga$ FC		$Ni_{1.24}Mn_{1.79}Ga_{0.98}$	5.8824(5)	162
$NiMn_2Ga$ RQ	6.75	$Ni_{1.05}Mn_{1.90}Ga_{1.05}$	5.9052(4)	146
$NiMn_2Ga$ FC		$Ni_{0.88}Mn_{2.14}Ga_{0.98}$	5.9022(5)	208

the crystallographic positions in a tetragonal lattice. These modulated structures help in lowering hysteresis losses and actuation fields leading to a better functionality of the Heusler alloy. Therefore, the observation of modulated structure in Mn_2NiGa increases its applicability considering its high magnetic ordering temperature and high martensitic transformation temperature. Theoretical calculations have also concurred with the experimental observations of modulated structures in the martensitic state [18]. Powder x-ray diffraction studies on Mn_2NiGa established a relation between the martensitic structure and the residual stress [19]. With increasing stress, the martensitic structure was shown to change from 7M monoclinic to tetragonal. These studies also showed the existence of the martensitic phase at room temperature which was above the transformation temperature of the alloy. The presence of the additional phase was also confirmed from neutron diffraction studies and it was shown to be present at all temperatures in the austenitic state [5]. Microstructure studies also reported the presence of additional structural phases. In addition, minor fraction of the martensitic phase was seen well above the transition temperature in both, the stoichiometric and off-stoichiometric Mn_2NiGa. These additional precipitates were identified as Mn-rich phases and were reported to disappear after annealing at 1123 K for 24 h [20].

The existence of modulated phases well above the martensitic transition temperature of Mn_2NiGa is quite interesting and needs to be understood. Recently, it has been shown that a similar alloy, Mn_2NiSn, phase separates upon temper annealing into Ni_2MnSn type Heusler and Mn_3Sn type $D0_{22}$ phases [21]. Similar phase segregation has been reported in several other Mn-rich Heusler alloys of the type $Ni_{50}Mn_{50-y}Z_y$ (Z = Ga, Sn, In, Sb) [22] EXAFS investigations on as-prepared and temper annealed $Ni_{50}Mn_{50-y}In_y$ alloys revealed existence of local phase separation of Heulser and $L1_0$ phases in all off-stoichiometric as-prepared compositions [23]. Such local phase separation is caused due to the stress caused by size difference between Mn and the substituted In atoms in $Ni_{50}Mn_{50-y}In_y$. Therefore, the presence of the modulated phases in Mn_2NiGa could also be stress-related. A question then arises if the stress affected structural correlations in Mn_2NiGa are responsible for the appearance of martensitic transformation at a higher temperature as compared to Ni_2MnGa by violating the so called e/a rule. To seek

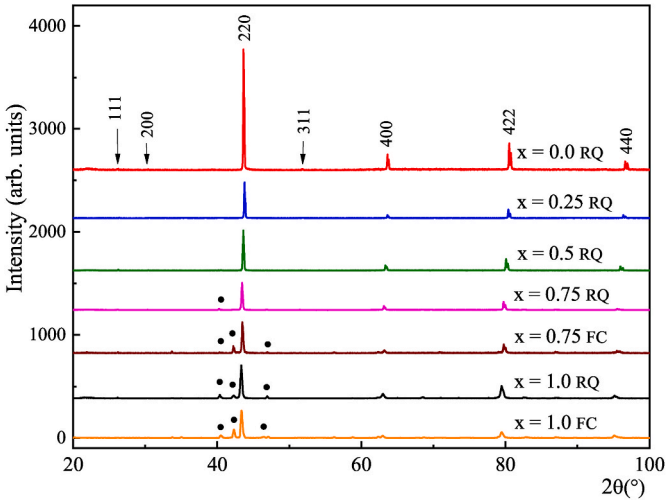

Fig. 2. XRD patterns of RQ $Ni_{(2-x)}Mn_{(1+x)}Ga$ (x = 0, 0.25, 0.5, 0.75 and 1)and FC x = 0.75 and 1 samples recorded at room temperature. The black dots indicate presence of impurity phases.

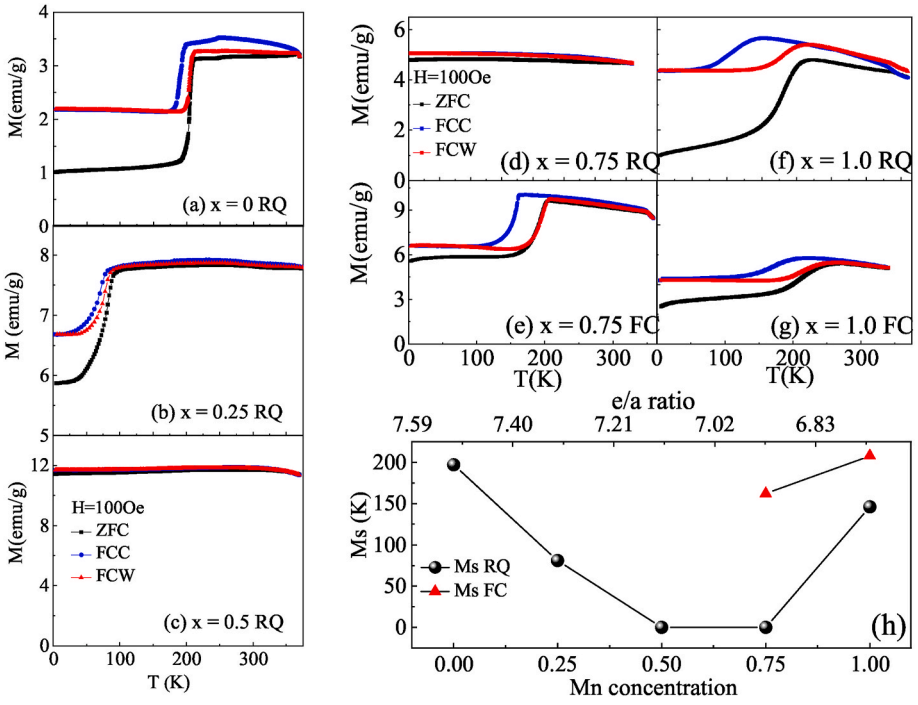

Fig. 1. (a–g) Plots of magnetization as a function of temperature measured in 100 Oe field during ZFC, FCC, and FCW cycles for the RQ and the FC alloys of composition $Ni_{2-x}Mn_{1+x}Ga$. (h) Variation of T_M as a function of x and e/a ratio in $Ni_{2-x}Mn_{1+x}Ga$.

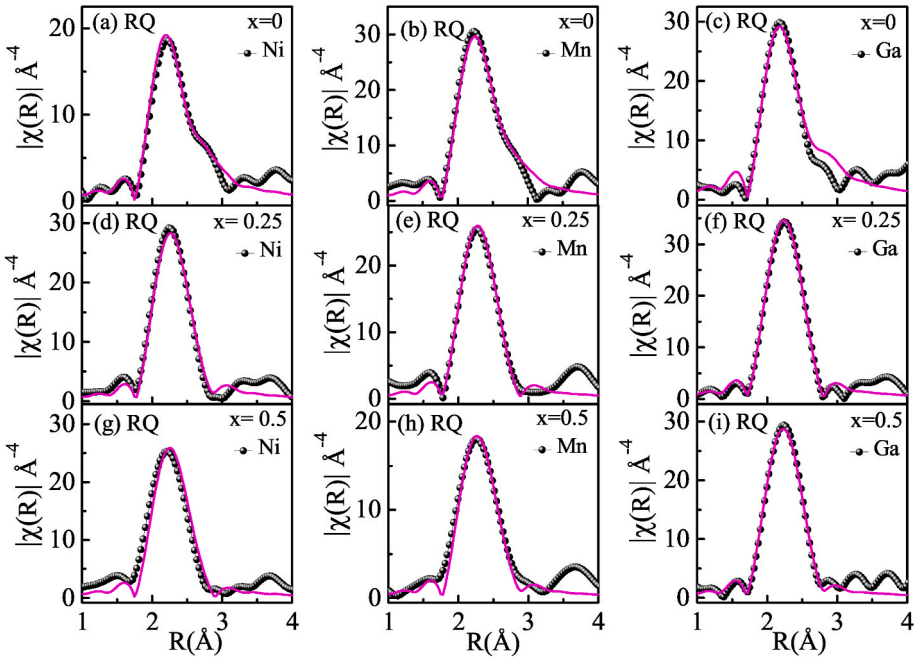

Fig. 3. Fourier transform magnitudes of k^3 weighted EXAFS recorded at 300K at the Ni, Mn and Ga K edges in Ni_2MnGa, $Ni_{1.75}Mn_{1.25}Ga$ and $Ni_{1.5}Mn_{1.5}Ga$ RQ alloys.

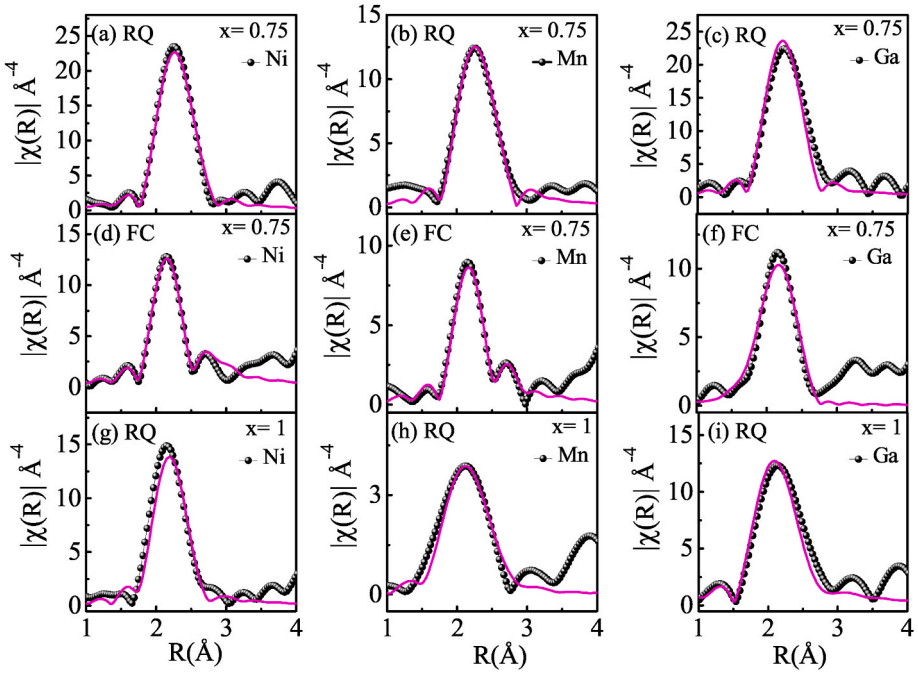

Fig. 4. The magnitude of Fourier transform of k^3 weighted Ni, Mn and Ga K edge EXAFS recorded at 300 K in RQ and FC alloy compositions, $Ni_{1.25}Mn_{1.75}Ga$ and RQ $NiMn_2Ga$.

answers to this question, we report studies on $Ni_{2-x}Mn_{1+x}Ga$ with $0 \leq x \leq 1$. The $L2_1$ structure (X_2YZ) of Ni_2MnGa consists of 8 Ni atoms occupying the X sites, 4 Mn atoms at the Y sites and 4 Ga atoms at the Z sites. The values of $x = 0$, 0.25, 0.5, 0.75 and 1 are so chosen to represent an incremental replacement of one Ni atom at a time and realize in Mn_2NiGa ($x = 1$). We also investigate the effect of different annealing treatments, rapid quenching versus furnace cooling, on the martensitic properties of these Mn-rich alloys.

2. Experimental

The polycrystalline samples were synthesized by arc melting the high purity (> 99.9%) elements, Ni, Mn and Ga in an argon atmosphere. The resulting beads were flipped and remelted three times to ensure homogeneity. The ingots were then cut into two halves using a low-speed diamond saw. While one of the halves was mechanically crushed into a fine powder for structural studies, the remaining half was sliced further into the smaller pieces that were used for other measurements. All of these pieces and the powder wrapped in tantalum foil were annealed at 800 °C for three days by encapsulating them in a quartz tube

Table 2
Near neighbour bond distances (R) and the mean-square disorder in the bond length (σ^2) obtained by simultaneous fitting of 300 K Ni, Mn and Ga K-edge EXAFS data for RQ, FC $Ni_{2-x}Mn_{1+x}Ga$ series. Uncertainties in the last digit are given in the parentheses.

Alloy	Ni–Mn		Ni–Ga		Ga–Mn		Ni–Ni		Mn–Ga		Mn–Mn	
	R (Å)	σ^2 (Å^2)	R (Å)	σ^2 (Å^2)	R (Å)	σ^2 (Å^2)	R (Å)	σ^2 (Å^2)	R (Å)	σ^2 (Å^2)	R (Å)	σ^2 (Å^2)
Ni_2MnGa RQ	2.510(1)	0.010(1)	2.5104 (1)	0.003 (1)	2.899(1)	0.012 (2)	2.899(1)	0.013(2)				
$Ni_{1.75}Mn_{1.25}Ga$ RQ	2.520 (10)	0.009(1)	2.539 (11)	0.009 (1)	2.924 (13)	0.016 (3)	2.892 (26)	0.018(5)				
$Ni_{1.5}Mn_{1.5}Ga$ RQ	2.525(3)	0.0104 (4)	2.546(8)	0.008 (1)	2.912(8)	0.017 (2)	2.923 (70)	0.023 (12)			2.765 (60)	0.009(9)
$Ni_{1.25}Mn_{1.75}Ga$ RQ	2.507 (11)	0.009(2)	2.545 (16)	0.009 (1)	2.967 (44)	0.012 (9)	2.902 (18)	0.017(3)	2.770 (134)	0.013 (16)	2.829 (22)	0.004(6)
$Ni_{1.25}Mn_{1.75}Ga$ FC	2.505(7)	0.011(1)	2.544 (12)	0.013 (2)	2.950 (25)	0.018 (4)	2.895 (21)	0.019(3)	2.716(27)	0.012(5)	2.732 (50)	0.011(9)
$NiMn_2Ga$ RQ	2.512 (16)	0.010(2)	2.529 (36)	0.012 (2)	2.950 (30)	0.015 (5)	2.897 (29)	0.020(5)	2.707(38)	0.012 (10)	2.871 (37)	0.004 (37)

Table 3
Values of near neighbour bond distances (R) and the mean-square disorder in the bond length (σ^2) obtained from simultaneous by the fitting of 30K Ni, Mn and Ga K-edge EXAFS for RQ, FC $Ni_{2-x}Mn_{1+x}Ga$ alloys. Figures in brackets signify variability in the last digit.

Alloy	Ni–Mn		Ni–Ga		Ga–Mn		Ni–Ni		Mn–Ga		Mn–Mn	
	R (Å)	σ^2 (Å^2)	R (Å)	σ^2 (Å^2)	R (Å)	σ^2 (Å^2)	R (Å)	σ^2 (Å^2)	R (Å)	σ^2 (Å^2)	R (Å)	σ^2 (Å^2)
Ni_2MnGa RQ	2.525(6)	0.005 (1)	2.507(3)	0.004 (1)	2.806(9)	0.002(1)	2.794 (12)	0.003(1)				
					3.035 (23)	0.002(2)	3.036 (29)	0.004(3)				
$Ni_{1.75}Mn_{1.25}Ga$ RQ	2.516(7)	0.004 (1)	2.531(9)	0.004 (1)	2.868 (14)	0.004(3)	2.856 (14)	0.003(2)				
					3.015 (19)	0.003(4)	3.020 (30)	0.003(2)				
$Ni_{1.5}Mn_{1.5}Ga$ RQ	2.513(4)	0.004 (1)	2.550(6)	0.004 (1)	2.920 (12)	0.001(2)	2.892 (29)	0.012(4)			2.795 (36)	0.0028 (4)
$Ni_{1.25}Mn_{1.75}Ga$ RQ	2.514 (11)	0.005 (1)	2.551 (16)	0.006 (1)	2.930 (30)	0.013(5)	2.910 (18)	0.013(3)	2.828 (265)	0.029 (50)	2.831 (22)	0.003(4)
$Ni_{1.25}Mn_{1.75}Ga$ FC	2.526 (13)	0.006 (2)	2.580 (12)	0.006 (1)	2.780(7)	0.018 (53)	2.780(7)	0.005(1)	2.670(36)	0.006(9)	2.787 (24)	0.001(4)
					3.005 (16)	0.025 (56)	3.005 (16)	0.006(1)				
$NiMn_2Ga$ RQ	2.512 (16)	0.006 (1)	2.529 (36)	0013(1)	2.950 (30)	0.013(5)	2.897 (29)	0.029 (21)	2.707(38)	0.008(4)	2.871 (37)	0.028 (11)

under a vacuum environment ($\geq 10^{-3}$ mbar) followed by rapid quenching in ice water (referred to as RQ). The alloy compositions with $x = 0.75$ and 1 were prepared and annealed again using the same procedure except instead of quenching, they were furnace cooled from 800 °C to room temperature (referred to as FC). The elemental compositions of the alloys were deduced from the energy dispersive x-ray (EDX) analysis and are reported in Table 1. Surface morphologies were examined by scanning electron microscopy. The micrographs on select samples are presented in the Supplementary information. Structural characterization was achieved by x-ray diffraction (XRD) studies on the annealed powders of the alloys at room temperature using Cu-Kα radiation ($\lambda = 1.5418$ Å) in the 2θ range of 20°–100°. Diffraction patterns were also recorded using synchrotron radiation of $\lambda = 0.6344$ Å at the BL beamline at the INDUS-2 synchrotron source. The diffraction patterns were Le Bail and Rietveld refined using the FULLPROF suite [24]. Magnetization measurements were performed on a vibrating sample magnetometer in an applied field of 100 Oe. The samples were cooled from 300 K down to the lowest temperature (3 K) in zero field, after which the field was applied and magnetization was measured during warming (ZFC) and subsequent cooling (FCC) and warming (FCW) cycles. Extended x-ray absorption fine structure (EXAFS) were recorded in transmission mode at Mn (6539 eV), Ni (8333 eV), and Ga (10367 eV) K-edges on the P65 beamline at PETRA III synchrotron source at T = 100 K and 300 K. The incident (I_0) and the transmitted (I) photon energies were simultaneously recorded using gas ionization chambers filled with appropriate mixtures. The thickness t of the absorbers were adjusted to obtain an absorption edge jump, $\Delta\mu t \leq 1$. EXAFS data were averaged over three to five scans at each temperature to minimize the statistical noise. The EXAFS signal was extracted and analyzed in the range of 3–14 Å^{-1} using the well-established procedures in the Demeter suite [25].

3. Results

In $Ni_{2-x}Mn_{1+x}Ga$, as the ratio of Ni to Mn changes from 2:1 ($x = 0$) to 1:2 ($x = 1$), the e/a ratio decreases linearly from 7.5 to 6.75. Ordinarily, this decrease in the e/a ratio should have resulted in a decrease in T_M. However, after the initial decrease of T_M from about 200 K for Ni_2MnGa to about 30 K in alloy with $x = 0.5$, T_M again rises to 270 K in $NiMn_2Ga$ [1]. To ascertain this behaviour of T_M in the present set of alloys, magnetization as a function of temperature, M(T) was recorded during the ZFC, FCC and FCW cycles in a field of 100 Oe. The M(T) curves for RQ and FC $Ni_{2-x}Mn_{1+x}Ga$ ($x = 0$, 0.25, 0.5, 0.75 and 1) alloys, in the temperature interval 3 K $\leq$ T $\leq$ 325 K, are presented in Fig. 1 (a – g). In the case of Ni_2MnGa ($x = 0$), magnetization recorded during the warming cycles (ZFC and FCW) displays a sharp decrease at 197 K and is termed as the martensitic start temperature $M_s = T_M$ (see Fig. 1(a)). The hysteresis in the transformation temperature during the warming and cooling (FCC) magnetization cycles confirms the first-order nature of the transition. Isothermal magnetization (not shown) recorded at 300 K confirms the ferromagnetic nature of the alloy which is in confirmation that the T_C of Ni_2MnGa is about 370 K. A similar behaviour is noted in

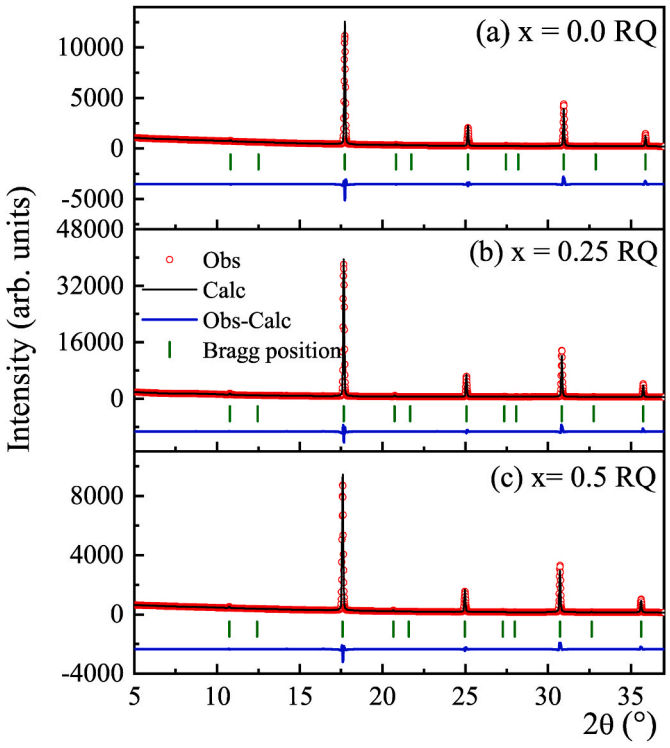

Fig. 5. Synchrotron x-ray diffraction patterns of $Ni_{2-x}Mn_{1+x}Ga$, x = 0, 0.25 and 0.5 RQ alloys.

the alloy with $x = 0.25$ with T_M at 81 K and T_C above 300 K (Fig. 1(b)). The RQ alloys with $x = 0.5$ and 0.75 display ferromagnetic nature and nearly invariant magnetization in the temperature interval of 3 K–325 K (Fig. 1(c) and (d)) implying the absence of martensitic transformation in these alloys. Martensitic transition reappears with further increase in x to 1 with $T_M = 162$ K (Fig. 1(f)). There is also a difference in the ZFC and FCC/FCW magnetization below martensitic transition temperature. This difference in the magnetization values could be ascribed to antisite disorder which can result in Mn–Mn antiferromagnetic interactions [19, 26] Though the transformation temperatures reported here are quite different from those observed earlier [1], the variation of T_M as a function of increasing Mn concentration is similar to that observed earlier [1]. The difference in temperatures could be due to different annealing heat treatments given to the alloys. Further, furnace cooling the alloys after annealing results in the appearance of martensitic transformation in the alloy with $x = 0.75$ (Fig. 1(e)) and an increase in T_M to 209 K in $x = 1$ (Fig. 1(g)). Furnace cooling of $x = 0.5$ did not result in any change in the observed characteristic of the RQ alloy. The values of T_M along with the elemental compositions obtained from EDX and the lattice constants of the cubic Heusler phase of the alloys are listed in Table 1. Fig. 1(h) displays a variation of T_M as a function of the excess Mn concentration, x and the e/a ratio. The variation is qualitatively similar to the one obtained earlier [1]. In particular, it displays an increase in T_M as the e/a ratio decreases from 6.9 to 6.75 (x increases from 0.75 to 1) in both RQ and FC alloys.

Fig. 2 shows the XRD patterns for RQ and FC $Ni_{2-x}Mn_{1+x}Ga$ ($x = 0$, 0.25, 0.5, 0.75 and 1.0) alloys that were recorded at room temperature. All the diffraction peaks can be indexed to face centred cubic $L2_1$ crystal structure with no detectable impurities. Weak impurity phases, in addition to the cubic Heusler phase, are visible in the diffraction patterns of both RQ and FC alloys with $x = 0.75$ and 1. The intensities of the impurity peaks appear to grow with increasing x and with the changes in heat treatment. Such impurity phases have been observed earlier and have been linked to the presence of residual stress in the alloys. Le Bail refinement of the diffraction patterns, presented in the Supplementary

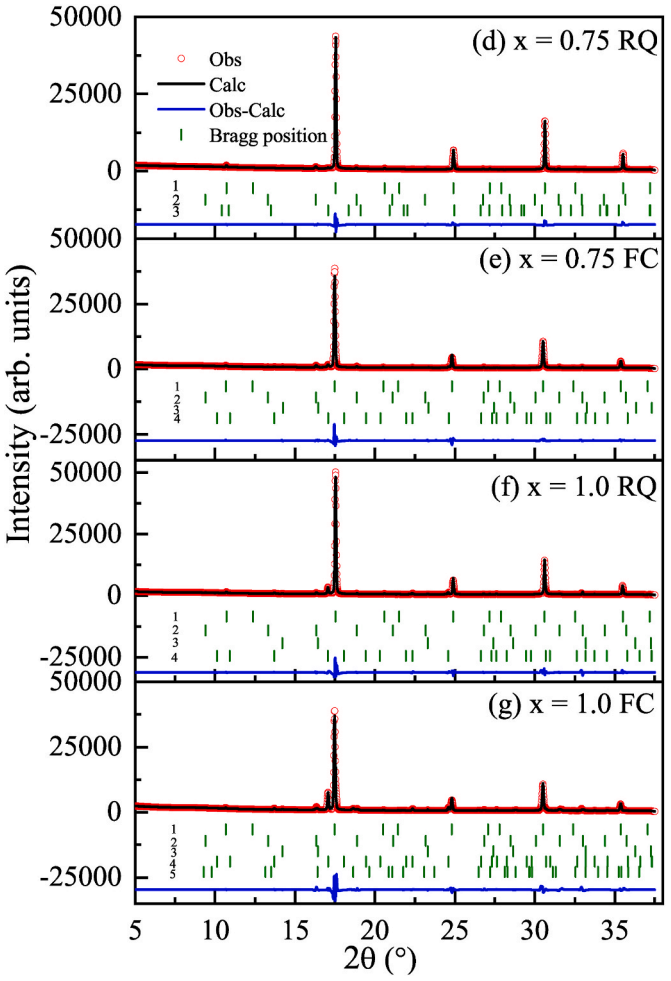

Fig. 6. Synchrotron x-ray diffractograms of RQ and FC alloy compositions, $Ni_{1.25}Mn_{1.75}Ga$ and $NiMn_2Ga$. Structural phases identified from Rietveld analysis are indicated by numerals, 1 - Fm3m, 2 - P4/mmm, 3- MnO, 4 - I4/mmm and 5 - Pm3 m.

Table 4
Phase fractions of constituent phases in $Ni_{1.25}Mn_{1.75}Ga$ and $NiMn_2Ga$ RQ and FC alloys.

Alloy	Phase Fractions			
	$L2_1$	$L1_2$	$D0_{22}$	$L1_0$
	$Fm\bar{3}m$	$Pm\bar{3}m$	$I4/mmm$	$P4/mmm$
$Ni_{1.25}Mn_{1.75}Ga$ RQ	80.47	11.23	8.30	–
$Ni_{1.25}Mn_{1.75}Ga$ FC[a]	79.99	3.72	9.80	–
$NiMn_2Ga$ RQ [a]	79.92	8.19	7.01	–
$NiMn_2Ga$ FC[a]	70.17	3.79	13.94	5.54

[a] The shortfall in the sum of phase fractions is made up by MnO impurity phase.

Information, helped in confirming the major structural phase to be $L2_1$ cubic and the impurity peaks seen in $x = 0.75$ and 1 alloys to belong to a 7M monoclinic phase in agreement with literature reports [19]. The cell constants of the cubic $L2_1$ cell were calculated (see Table 1) and also found to be in close agreement with literature values [1,12,15].

Could the presence of impurity phases have any role to play in the behaviour of T_M as a function of the e/a ratio? To further investigate this aspect, EXAFS was recorded at 300 K and 100 K at the Ni, Mn and Ga K edges to study the changes in the local structure of these constituent atoms in their austenitic and martensitic phases. EXAFS data in the k

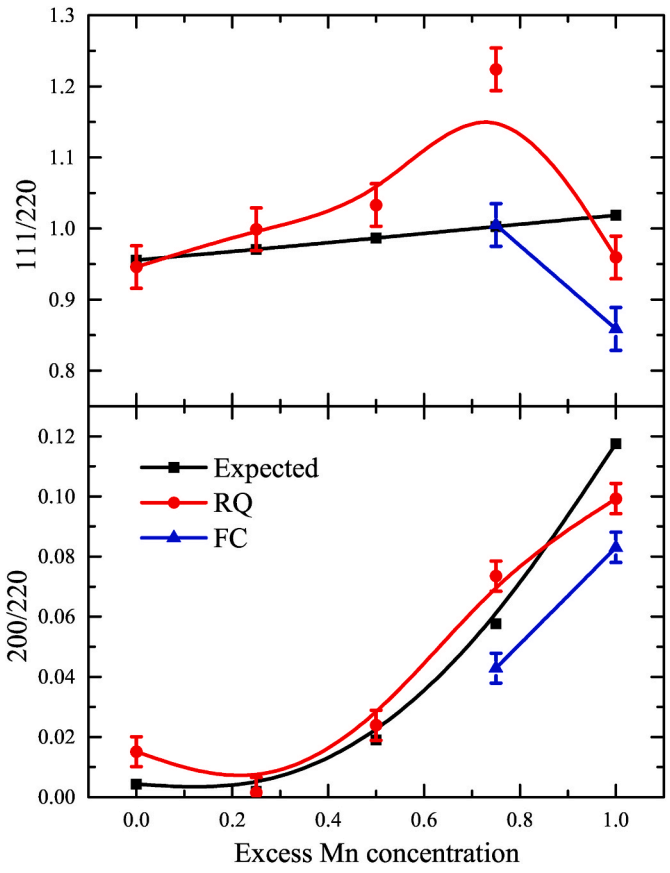

Fig. 7. Variation of calculated and observed intensity ratios, $I_{(111)}/I_{(220)}$ and $I_{(200)}/I_{(220)}$ as a function of excess Mn concentration (x).

range of 3–14 Å^{-1} and R range of 1–3 Å, at all the three edges were fitted together with a common structural models used earlier in Ref. [15]. Fitting EXAFS data at all three edges together not only reduces the number of free parameters but also increases the reliability in obtained values of bond distances. The fit consists of four correlations, the nearest neighbour Ni–Mn and Ni–Ga, and the next nearest neighbour Ni–Ni and Mn–Ga. A fit procedure designed to include the structural constraints yielded good fits to all three data sets in Ni_2MnGa ($x = 0$). Figs. 3 and 4 display Fourier transform magnitude of the k^3 weighted $\chi(k)$ spectra recorded at the Ni, Mn and Ga edges respectively for all the $Ni_{2-x}Mn_{1+x}Ga$ RQ and FC alloys.

The increase in the value of x implies progressive occupation of the Ni sites by Mn. This results in three new correlations, Mn_X–Mn, Mn_X–Ga and Mn_X–Ni (Mn_X corresponds to Mn occupying the X sublattice of X_2YZ Heusler structure). In $Ni_{1.75}Mn_{1.25}Ga$ ($x = 0.25$) however, the data at all three edges could be fitted without including any of the three new correlations. Since the electronic density differences between Mn (Z = 25), Ni (Z = 28) and Ga (Z = 31) are within $\Delta Z = \pm 5$, it would be difficult to distinguish between them as scatterers at the same distance. But to get a good fit, the structural constraints imposed by the $L2_1$ structure had to be relaxed. This is evident from the values of bond distances listed in Tables 2 and 3 where Ni–Mn and Ni–Ga distances are not equal. This difference in nearest neighbour distances could be due to structural strain caused by the Mn atom occupying Ni (X) sites.

With a further increase in x, the effect of Mn substitution became even more evident. In $x = 0.5$ the Mn and Ga EXAFS data could not be fitted with the above structural model even though its crystal structure is cubic. The Mn_X–Mn correlation had to be included in the fitting procedure but its bond distance was found to be ~ 2.76 Å which is larger than the expected value of about 2.52 Å. For higher values of $x = 0.75$ and 1, both Mn_X–Mn and Mn_X–Ga correlations had to be included in the fitting procedure to obtain good fits. The bond distances of both these correlations (see Tables 2 and 3) were larger than their expected values pointing to a segregation of structural defects rich in Mn. Further support to the segregation of structural defects comes from a consistent decrease in the amplitude of Ni, Mn and Ga EXAFS oscillations (see Supplementary Information) with an increase in x. Such a decrease of EXAFS amplitude could be ascribed to an out of phase addition of contributions to the EXAFS signal from the defect phase and the Heusler phase. The presence of a defect phase rich in Mn is also supported from the observation of Mn-rich precipitates in the polycrystalline alloys of $Mn_{2+x}NiGa_{1-x}$ [20]. The defects, however, do not seem to be responsible for the absence of martensitic transition in $x = 0.5$ and 0.75 as they are also present in the martensitic alloys, $x = 1$ (RQ) and $x = 0.75$ (FC).

The previous structural studies reporting impurity phases in Mn_2NiGa alloys have suggested them to be modulated 5M or 7M phases arising most probably due to residual stress [5,19]. However, such modulated structures do not account for the nearest neighbour distances of about 2.7–2.8 Å [12]. The other Mn-rich defect phase possible is Mn_3Ga. Both the tetragonal and cubic phases of Mn_3Ga consist of nearest neighbour Mn–Mn and Mn–Ga bonds at 2.7 and 2.8 Å. To explore the possibility of existence of Mn_3Ga phases as defect phases, refinement of synchrotron x-ray diffraction patterns of all the $Ni_{2-x}Mn_{1+x}Ga$ (both RQ and FC alloys) was carried out. The diffraction patterns were recorded using x-rays of energy ~ 19.5 KeV which is well above the absorption edge energies of the constituent elements. The refined patterns along with the difference spectra and the constituent phase markers are presented in Figs. 5 and 6. As deciphered from the lab XRD pattern, the crystal structures of the alloys with $x = 0$, 0.25 and 0.5 at room temperature are cubic $L2_1$ type with no other impurity phases (Fig. 5). Inclusion of cubic ($Fm\bar{3}m$) and tetragonal ($I4/mmm$) structures of Mn_3Ga along with the cubic Heusler structure reproduces the diffraction patterns of RQ and FC $Ni_{2-x}Mn_{1+x}Ga$ alloys with $x = 0.75$ and 1.0 quite well (Fig. 6). This indicates that the longer Mn–Ga and Mn–Mn nearest neighbour distances obtained from EXAFS analysis indeed arise from a Mn_3Ga type defect phase. The phase fractions of the constituent phases in $Ni_{1.25}Mn_{1.75}Ga$ and $NiMn_2Ga$ are tabulated in Table 4.

Mn_3Ga type phase in Mn-rich $Ni_{2-x}Mn_{1+x}Ga$ alloys can segregate via an antisite disorder between Mn and Ga (Y and Z) sites. To confirm the presence of such a disorder we analyse the intensity variations of (111) and (200) superlattice reflections with that of the principal (220) reflection with an increase in the value of x. The intensity ratios, $I_{(111)}/I_{(220)}$ and $I_{(200)}/I_{(220)}$ provide information regarding the antisite disorder in the alloy. The $I_{(200)}/I_{(220)}$ provides information exclusively on occupancy disorder between X and Y/Z sublattices of the X_2YZ Heusler alloy. On the other hand, $I_{(111)}/I_{(220)}$ is affected by the disorder between Y and Z sublattices as well as the disorder between X and Y/Z sublattices [27].

Fig. 7 displays the two observed ratios, $I_{(111)}/I_{(220)}$ and $I_{(200)}/I_{(220)}$ in panels (a) and (b) respectively along with the calculated ratios for both RQ and FC alloys. The calculated ratio represents the intensity ratio for an ordered $L2_1$ lattice of the type $Ni_{2-x}Mn_xMnGa$ where $x = 0$, 0.25, 0.5, 0.75 and 1.0. It can be seen that both calculated and observed $I_{(200)}/I_{(220)}$ ratios increase with the value of x. This is expected due to the increasing replacement of Ni by Mn atoms. Both the calculated and the observed ratios scale together in all RQ alloys up to $x = 0.75$. A decrease is seen in the observed ratio as compared to the calculated value for $x = 1.0$. The ratio of observed intensities further decreases with respect to the calculated values for the two FC alloys. Such a behavior hints at lower site disorder due to furnace cooling rather than quenching them from high temperature.

The $I_{(111)}/I_{(220)}$ ratio is expected to show minimum variation as a function of x as there is no disorder expected between Y and Z sublattices due to the substitution of Mn for Ni at the X sites. The same is also reflected in the variation of the calculated ratio in Fig. 7(a). Surprisingly the observed ratios display large deviations from the calculated values for alloys with $x \geq 0.5$. In the case of RQ alloys, the $I_{(111)}/I_{(220)}$ ratio

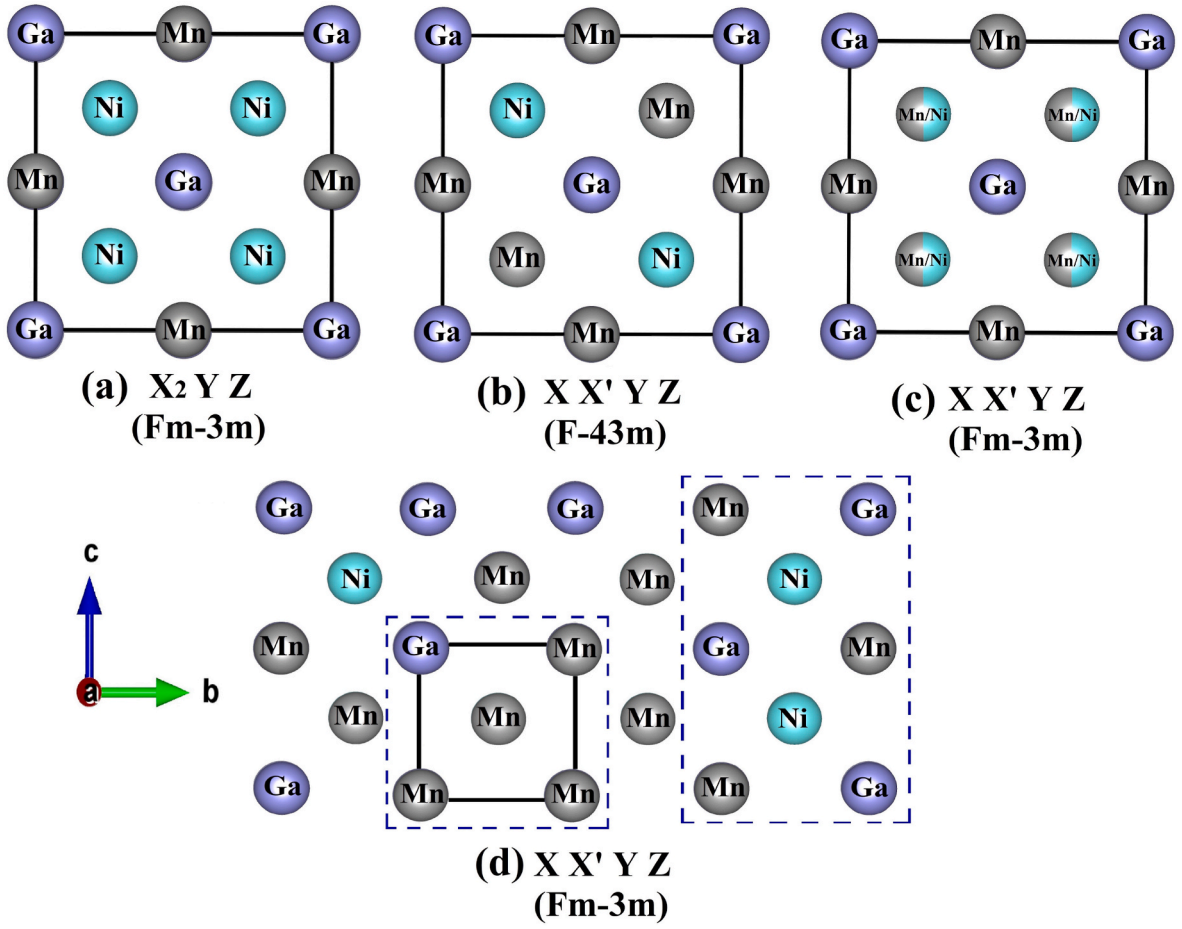

Fig. 8. Two dimensional projections showing X_2YZ, ordered XX'YZ, disordered XX'YZ and the possible segregation of Mn_3Ga type defects due to antisite disorder in XX'YZ.

increases steadily with x and reaches a maximum around $x = 0.75$ and then decreases sharply with further increase in the value of x. In the case of the two FC alloys, the intensity ratios are further affected and are much lower than their RQ counterparts.

4. Discussion

Despite a reduction of the e/a ratio upon substituting Ni by Mn in Ni_2MnGa, the martensitic transition temperature increases after the initial decrease. This has been an unsolved puzzle challenging the so called e/a rule. In Ni–Mn-Ga Heulser alloys, irrespective of the alloy stoichiometry, the martensitic transformation temperature scales with the e/a ratio [11]. The only few exceptions are Mn_2NiGa and its derivatives. The main objective of this work is to understand this violation of the e/a rule.

Structurally, Mn_2NiGa has always shown presence of minor impurity phases and have been assigned to stress -induced modulated martensitic phases [5,19]. Its martensitic transition temperature is also sensitive to the thermal heat treatment given to the alloys [20]. Here too, the furnace cooled alloys display higher T_M as compared to their quenched counterparts. Local structural studies of the Ni, Mn and Ga, however, showed presence of long Mn–Mn and Mn–Ga bond distances which could not be assigned to near-neighbour distances in $L2_1$ Heusler structure or the modulated martensitic structures reported for Ni–Mn-Ga alloys. These distances were found to close the Mn–Mn and Mn–Ga distances in Mn_3Ga cubic and tetragonal phases and the same was further confirmed from the refinement of synchrotron x-ray diffraction patterns.

Segregation of Mn_3Ga phases in the Mn_2NiGa Heusler structure is possible if there is an antisite disorder between the Y and Z sublattices of the X_2YZ Heusler structure. This possibility is schematically explained in Fig. 8. The $L2_1$ structure of the X_2YZ Heusler alloy is an ordered combination of two B2 lattices XY and YZ (Fig. 8(a)) crystallizing in a face-centred cubic lattice. Replacing X with X′ can lead to several possible scenarios of higher-order or antisite disorder. An ordering of X and X′ atoms and giving rise to a Hg_2CuTi type structure with $F\bar{4}3m$ space group (Fig. 8(b)). Without this X X′ order the structure remains $L2_1$ (Fig. 8(c)) and also supports partial disorder between the constituent sub-lattices as shown in Fig. 8(d). A disorder between Y and Z sublattices in absence of order between X and X' atoms can lead to segregation of Mn_3Ga type defect phase and a Heulser phase. Mn_3Ga possesses either a cubic or tetragonal structure with nearest neighbour distances larger (2.7 Å to 2.8 Å) than those in the cubic Heusler alloy (~ 2.52 Å). This explains the observation of larger Mn–Ga and Mn–Mn bond distances from Mn and Ga EXAFS studies. It may be noted that these longer bond distances are especially seen in $Ni_{2-x}Mn_{1+x}Ga$ alloys with $x = 0.75$ and 1.0.

In the present $Ni_{2-x}Mn_{1+x}Ga$ alloys, the variation of intensity ratios of superlattice to principal reflections, especially I_{111}/I_{220} support the existence of antisite disorder between all three sublattices of the Heusler structure. The agreement between the observed and calculated I_{200}/I_{220} ratio indicates the substitution of Mn for Ni. Except for the quenched $NiMn_2Ga$ and the two FC alloy compositions ($x = 0.75$ and 1), there is a near-perfect agreement between the calculated and the observed I_{200}/I_{220} ratio. Interestingly, in these alloys, the martensitic transition temperature scales with the e/a ratio. The martensitic transition is present in

the RQ $NiMn_2Ga$ and the FC $Ni_{1.25}Mn_{1.75}Ga$ and $NiMn_2Ga$ alloys and in all these three compositions significant deviation between the observed and calculated values of I_{200}/I_{220} is observed. The lower values of the observed intensity ratio indicate the formation of the Heusler phase richer in Ni as compared to the expected composition. This hypothesis also supports the segregation of Mn_3Ga type impurity phases. Formation of Ni-rich Heusler phase and the Y – Z sublattice disorder needed for segregation of Mn_3Ga type phases is further supported by the higher observed I_{111}/I_{220} ratio as compared to the calculated values. Higher I_{111}/I_{220} ratio is possible in the case of occupancy disorder between X (Ni) and Y(Mn) sublattices. It may also be noted that the ratio starts deviating from $x = 0.5$, the composition in which longer Mn–Mn bonds were first observed from the EXAFS analysis. Thus the considerably different observed intensity ratios of I_{111}/I_{220} and I_{200}/I_{220} indicate the formation of the Heusler phase richer in Ni than the expected composition and therefore higher e/a ratio. The scaling of T_M with e/a ratio in Ni–Mn-Ga Heusler alloys is well known. Therefore, the segregation of Ni-rich Heusler phases and Mn_3Ga type phases due to antisite disorder in $Ni_{2-x}Mn_{1+x}Ga$ alloys appears to be the primary reason for the increase in martensitic transition temperature of these alloys.

5. Conclusions

The increase of the martensitic transition temperature in $Ni_{2-x}Mn_{1+x}Ga$ alloys despite a decrease in the e/a ratio can be ascribed to a site occupancy disorder in the Heusler alloy that results in segregation of Mn_3Ga type defect phase and an Heusler phase that is rich in Ni. Substitution of Mn for Ni results in Mn–Mn nearest neighbour interactions which perpetrate Mn_3Ga type defects. These defects segregate in impurity phases with increasing substitution of Ni by Mn. The Ni-rich Heusler phases have a comparatively higher e/a ratio and appear to be the main cause of higher T_M in Mn_2NiGa as compared to Ni_2MnGa.

Authorship statement

Category 1: Conception and design of study: K. R. Priolkar, S. V. Malik; acquisition of data: S. V. Malik, E. T. Dias, P. D. Babu, V. Srihari; analysis and/or interpretation of data: S. V. Malik, E. T. Dias, K. R. Priolkar.

Category 2: Drafting the manuscript: S. V. Malik, K. R. Priolkar; revising the manuscript critically for important intellectual content: K. R. Priolkar, E. T. Dias, P. D. Babu, V. Srihari.

Category 3: Approval of the version of the manuscript to be published (the names of all authors must be listed): S. V. Malik, E. T. Dias, P. D. Babu, V. Srihari, K. R. Priolkar.

Data availability

The data that support the findings of this study are available from the corresponding author upon reasonable request.

Declaration of competing interest

The authors declare that they have no known competing financial interests or personal relationships that could have appeared to influence the work reported in this paper.

Acknowledgements

K.R.P. and S.V.M. acknowledge the Science and Engineering Research Board (SERB) for the financial assistance under project EMR/2017/001437 and the travel support from the Department of Science and Technology, Govt. of India within the framework of India DESY collaboration. We thank DESY (Hamburg, Germany), a member of Helmholtz Association HGF, for the provision of experimental facilities. Parts of this research were carried out at PETRA III and we thank Edmund Welter and Ruidy Nemausat for experimental assistance. Beamtime was allocated for the proposal (I-20180679).

Appendix A. Supplementary data

Supplementary data to this article can be found online at https://doi.org/10.1016/j.intermet.2022.107613.

References

[1] G.D. Liu, J.L. Chen, Z.H. Liu, X.F. Dai, G.H. Wu, B. Zhang, X.X. Zhang, Appl. Phys. Lett. 87 (26) (2005), 262504.
[2] S. Singh, S. Esakki Muthu, A. Senyshyn, P. Rajput, E. Suard, S. Arumugam, S. Barman, Appl. Phys. Lett. 104 (5) (2014) 51905.
[3] S. Singh, R. Rawat, S.E. Muthu, S. D'Souza, E. Suard, A. Senyshyn, S. Banik, P. Rajput, S. Bhardwaj, A. Awasthi, et al., Phys. Rev. Lett. 109 (24) (2012), 246601.
[4] D. Schaefer, A. de Oliveira, P. de Camargo, J. Varalda, W. Schreiner, D. Mosca, Intermetallics 91 (2017) 22–30, https://doi.org/10.1016/j.intermet.2017.08.001 [link]. URL, https://www.sciencedirect.com/science/article/pii/S0966979 51730211X.
[5] P. Brown, T. Kanomata, K. Neumann, K. Neumann, B. Ouladdiaf, A. Sheikh, K. Ziebeck, Atomic and magnetic order in the shape memory alloy mn2niga, J. Phys. Condens. Matter 22 (50) (2010), 506001.
[6] S. Paul, B. Sanyal, S. Ghosh, First-principles study of the lattice instabilities in mn2nix(x= al, ga, in, sn) magnetic shape memory alloys, J. Phys. Condens. Matter 27 (3) (2014), 035401, https://doi.org/10.1088/0953-8984/27/3/035401.
[7] J. Bai, J. Wang, S. Shi, X. Liang, Y. Yang, H. Yan, X. Zhao, L. Zuo, Y. Zhang, C. Esling, Theoretical prediction of structural stability, elastic and magnetic properties for mn2niga alloy, Mod. Phys. Lett. B 35 (10) (2021), 2150231, https://doi.org/10.1142/S0217984921502316 arXiv:.
[8] S.W. D'Souza, T. Roy, S.R. Barman, A. Chakrabarti, Magnetic properties and electronic structure of mn–ni–ga magnetic shape memory alloys, J. Phys. Condens. Matter 26 (50) (2014), 506001, https://doi.org/10.1088/0953-8984/26/50/506001.
[9] K. Ullakko, J.K. Huang, C. Kantner, R.C. O'Handley, V.V. Kokorin, Large magnetic-field-induced strains in ni2mnga single crystals, Appl. Phys. Lett. 69 (13) (1996) 1966–1968, https://doi.org/10.1063/1.117637, arXiv:.
[10] L. Righi, F. Albertini, G. Calestani, L. Pareti, A. Paoluzi, C. Ritter, P.A. Algarabel, L. Morellon, M. Ricardo Ibarra, J. Solid State Chem. 179 (11) (2006) 3525–3533.
[11] J. Pons, V. A. Chernenko, R. Santamarta, E. Cesari, Crystal structure of martensitic phases in Ni-Mn-Ga shape memory alloys, Acta Mater. 3027–3038.
[12] L. Righi, F. Albertini, E. Villa, A. Paoluzi, G. Calestani, V. Chernenko, S. Besseghini, C. Ritter, F. Passaretti, Acta Mater. 56 (2008) 4529–4535.
[13] L. Righi, F. Albertini, L. Pareti, A. Paoluzi, G. Calestani, Acta Mater. 55 (15) (2007) 5237–5245.
[14] S.R. Barman, S. Banik, A. Chakrabarti, Structural and electronic properties of Ni_2MnGa, Phys. Rev. B 72 (18) (2005), 184410, https://doi.org/10.1103/PhysRevB.72.184410.
[15] P.A. Bhobe, K.R. Priolkar, P.R. Sarode, Phys. Rev. B 74 (2006), 224425.
[16] H. Luo, F. Meng, Z. Feng, Y. Li, W. Zhu, G. Wu, X. Zhu, C. Jiang, H. Xu, J. Appl. Phys. 107 (1) (2010) 13905.
[17] G. Liu, X. Dai, S. Yu, Z. Zhu, J. Chen, G. Wu, H. Zhu, J.Q. Xiao, Phys. Rev. B 74 (5) (2006) 54435.
[18] A. Kundu, M.E. Gruner, M. Siewert, A. Hucht, P. Entel, S. Ghosh, Interplay of phase sequence and electronic structure in the modulated martensites of mn2NiGa from first-principles calculations, Phys. Rev. B 96 (2017) 64107, https://doi.org/10.1103/PhysRevB.96.064107.
[19] S. Singh, M. Maniraj, S. D'Souza, R. Ranjan, S. Barman, Appl. Phys. Lett. 96 (8) (2010) 81904.
[20] J. Zhang, W. Cai, Z. Gao, J. Sui, Scripta Mater. 58 (9) (2008) 798–801.
[21] S. V. Malik, E. T. Dias, A. K. Nigam, K. R. Priolkar, J. Phys. D Appl. Phys.doi: 10.1088/1361-6463/ac4b59.
[22] A. Cakir, M. Acet, M. Farle, Sci. Rep. 6 (2016) 28931.
[23] R. Nevgi, E.T. Dias, K.R. Priolkar, Phys. Rev. B 104 (2021) 54101.
[24] J. Rodríguez-Carvajal, T. Roisnel, Physica B 192 (1993) 55–69.
[25] B. Ravel, M. Newville, J. Synchrotron Radiat. 12 (4) (2005) 537–541.
[26] A. Çakır, M. Acet, L. Righi, F. Albertini, M. Farle, Characteristics of 5m modulated martensite in ni-mn-ga magnetic shape memory alloys, AIP Adv. 5 (9) (2015) 97222, https://doi.org/10.1063/1.4932233, arXiv:.
[27] Y. Takamura, R. Nakane, S. Sugahara, J. Appl. Phys. 105 (2009) 7B109.